Complex Precipitate Engineering for High-Temperature Stability in Additively Manufactured FeCrAl Alloys

Omer Cakmak[a], Hwasung Yeom[a,b], Jung-Wook Cho[a,b*]
[a]*Division of Advanced Nuclear Engineering, Pohang University of Science and Technology (POSTECH), Pohang, 37673, Republic of Korea*
[b]*Graduate Institute of Ferrous & Eco Materials Technology, Pohang University of Science and Technology (POSTECH), Pohang, 37673, Republic of Korea*

[*]*Corresponding author: jungwook@postech.ac.kr*

***Keywords: Thermal Exposure, Complex Precipitates, Microstructure, Mechanical Properties, LPBF.**

1. Introduction

Structural materials employed in nuclear systems are required to tolerate extreme service conditions, including elevated temperatures, intense radiation exposure, and highly corrosive environments. Consequently, these materials must exhibit a combination of essential properties, such as low thermal expansion, high creep resistance, strong radiation tolerance, and excellent corrosion resistance [1]. In this context, FeCrAl-based nitride dispersion-strengthened (NDS) and oxide dispersion-strengthened (ODS) alloys have emerged as promising candidates owing to their outstanding high-temperature mechanical performance, superior oxidation and corrosion resistance, and enhanced irradiation stability [2]. The incorporation of nanoscale nitride and oxide precipitates plays a crucial role in strengthening these alloys by hindering dislocation motion through dispersion strengthening, thereby significantly improving their elevated-temperature strength and long-term microstructural stability. Furthermore, the addition of alloying elements such as Ti and Y_2O_3 facilitates the formation of core–shell-type complex precipitates. Notably, the presence of complex oxide–nitride precipitates has been demonstrated to substantially enhance multiple material properties, including oxidation and corrosion resistance, as well as resistance to radiation-induced degradation [3,4].

The fabrication of FeCrAl alloys by Laser Powder Bed Fusion (LPBF), an additive manufacturing process, provides several notable advantages. In particular, LPBF enables precise control of the processing atmosphere, which facilitates the in-situ formation of secondary phases such as nitrides and oxides. The homogeneous distribution of these nanoscale precipitates within the matrix contributes to significant improvements in mechanical performance, including enhanced hardness, strength, wear resistance, creep resistance, and corrosion resistance, thereby enabling the design of materials with properties tailored for specific service requirements [5,6].

Microstructural evolution plays a decisive role in governing the high-temperature performance of alloys. Accordingly, a thorough understanding of the effects of thermal exposure duration on precipitate evolution, microstructural stability, and mechanical behavior is essential for tailoring material properties to meet application-specific demands. In this work, a Fe–12Cr–6Al–1Ti–0.25Y_2O_3 alloy was initially fabricated by LPBF under a nitrogen-rich (N_2) atmosphere to promote the in-situ formation of nitride precipitates. The influence of subsequent thermal exposure on precipitate characteristics, microstructural evolution, and mechanical properties was then systematically examined.

2. Experimental Methods

Fe–12Cr–6Al and Ti powders were supplied by MK Co. (South Korea) and produced by gas atomization. The particle size ranges of the Fe–12Cr–6Al and Ti powders were 15–45 μm and 5–15 μm, respectively. Y_2O_3 nanopowders, also obtained from MK Co., exhibited particle sizes in the range of 50–100 nm. The powder mixture was prepared by blending Fe–12Cr–6Al powder with 1 wt.% Ti and 0.25 wt.% Y_2O_3 using a high-speed mixer (KM Tech Co., South Korea) operated at 10,000 rpm for 6 min to achieve a homogeneous distribution. The samples were printed using an L-PBF machine (Metalsys-250, WINFORSYS) in a nitrogen (N_2) atmosphere. The LPBF process was performed using a laser power of 200 W, a scanning speed of 400 mm s^{-1}, a layer thickness of 30 μm, and a hatch spacing of 100 μm, with a 90° rotation applied between successive layers. Cuboidal specimens with dimensions of 30 × 10 × 10 mm^3 were fabricated for subsequent high-temperature testing. For each experimental condition, three samples were prepared and subjected to thermal exposure. Heat treatments were carried out in air at 1200 °C for durations of 1 h and 10 h. Following thermal exposure, the specimens were removed from the furnace and allowed to cool naturally in air. The cross-sectional morphology, size distribution, and chemical composition of nitride precipitates were characterized using a field-emission scanning electron microscope (SEM; JSM-7900F, JEOL). For each condition, tensile tests were performed on three dog-bone–shaped specimens with a gauge length of 6.4 mm and a gauge width of 2.5 mm. The specimens were

precisely machined from the additively manufactured material along the build direction. Room-temperature tensile properties were evaluated using a universal testing machine (Instron-582, INSTRON) at a constant strain rate of 10^{-3} s^{-1}. Accurate strain measurement during testing was achieved using a three-dimensional digital image correlation (DIC) system (ARAMIS M12, GOM, Germany).

3. Results and discussion

3.1 Influence of Thermal Exposure Time on Precipitate Evolution

SEM was used to investigate the effect of thermal exposure duration on the morphology and distribution of in-situ formed nanoscale precipitates in Fe–12Cr–6Al–1Ti–0.25Y_2O_3 alloys under as-built and high-temperature–exposed conditions (Fig. 1). In the as-built state (Fig. 1a), SEM–EDS mapping revealed a uniform distribution of TiN precipitates throughout the matrix, along with nanoscale Y-rich particles. After 1 h of thermal exposure at 1200 °C (Fig. 1b), TiN remained the dominant phase, while additional Y_2O_3 and Al_2O_3 precipitates were observed. SEM–EDS analysis further indicated preferential nucleation of TiN on Y_2O_3 particles, suggesting that Y_2O_3 acts as an effective heterogeneous nucleation site [2]. Following 10 h of thermal exposure (Fig. 1c), TiN precipitates continued to dominate the microstructure, accompanied by the formation of complex Al–Y–O oxide precipitates. Overall, the precipitate population evolved from TiN and Y-rich particles in the as-built condition to TiN, Al_2O_3, and TiN@Y_2O_3 core–shell structures after 1 h, and finally to TiN and Al–Y–O oxides after 10 h of exposure.

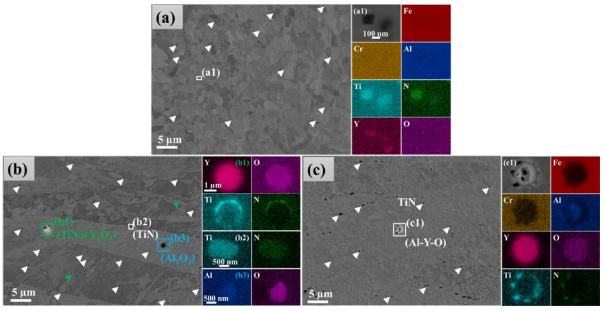

Fig.1. Backscattered electron (BSE) images and corresponding EDS elemental maps of the Fe–12Cr–6Al–1Ti–0.25Y_2O_3 alloy in the (a) as-built condition, (b) after 1 h of thermal exposure, and (c) after 10 h of thermal exposure at 1200 °C.

3.2 Microstructural Evolution as a Function of Thermal Exposure Duration

Fig. 2 presents a comparative analysis of the microstructural evolution of the Fe–12Cr–6Al–1Ti–0.25Y_2O_3 alloy, illustrating the effects of thermal exposure on grain orientation, morphology, and size. The inverse pole figure (IPF-X) map of the as-built sample is shown in Fig. 2a, revealing the initial grain structure along the scan direction. After 1 h of thermal exposure at 1200 °C (Fig. 2b), the alloy exhibited minimal changes in grain orientation and morphology, indicating a high degree of microstructural stability under short-term thermal exposure. In contrast, prolonged exposure for 10 h (Fig. 2c) resulted in evident grain growth and the onset of recrystallization. Kernel average misorientation (KAM) maps (Fig 2. (a1,b1,c1), which reflect local lattice distortions and internal strain, revealed a relatively uniform misorientation distribution in the as-built condition, consistent with the fine microstructure produced by rapid LPBF cooling (~10^6 °C s^{-1}) [7]. After 10 h of thermal exposure (Fig. 2(c1)), grain coarsening and irregular grain morphologies were observed, accompanied by localized regions of elevated misorientation, indicating thermally activated recovery and recrystallization. Quantitatively, the average grain size increased by approximately 4 μm after 1 h (Fig. 2(b2)) and by 7 μm after 10 h (Fig. 2(c2)) of thermal exposure compared to the as-built condition.

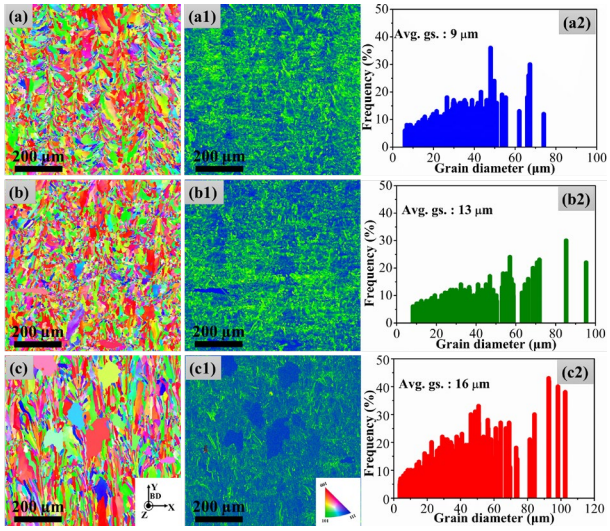

Fig.2. Scan direction IPF-X maps, KAM Maps, and grain size distribution analysis results of the Fe–12Cr–6Al–1Ti–0.25Y_2O_3 alloy in the (a,a1,a2) as-built condition, (b,b1,b2) after 1 h of thermal exposure, and (c,c1,c2) after 10 h of thermal exposure at 1200 °C.

3.3 Mechanical Property Evolution with Thermal Exposure Duration

Fig. 3 summarizes the mechanical properties of the Fe–12Cr–6Al–1Ti–0.25Y_2O_3 alloy in the as-built condition and after thermal exposure at 1200 °C for 1 h and 10 h. Following 1 h of thermal exposure, the yield strength (YS) and ultimate tensile strength (UTS) decreased from 461 MPa to 378 MPa and from 680 MPa to 551 MPa, respectively, while the elongation to failure increased from 26% to 36%. Extending the

exposure time to 10 h resulted in a further reduction in YS and UTS to 328 MPa and 451 MPa, respectively. The observed strength degradation after thermal exposure is primarily attributed to grain coarsening, which reduces grain boundary strengthening, as well as to a decrease in dislocation density [8]. In contrast, the enhanced ductility observed after 1 h of thermal exposure is likely associated with reduced dislocation density, which facilitates plastic deformation [9].

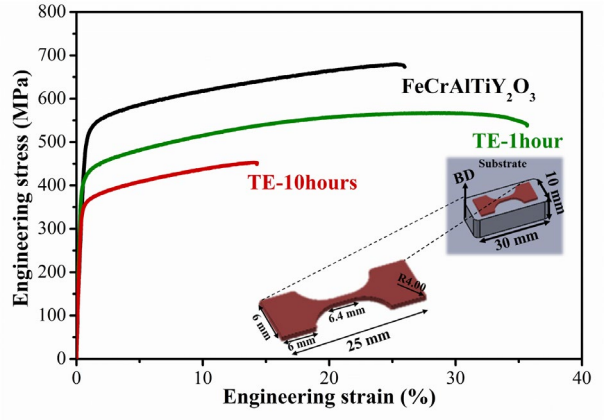

Fig.3. Tensile stress–strain curves of Fe–12Cr–6Al–1Ti–0.25Y_2O_3 samples in the as-built condition, after 1 hour of thermal exposure, and after 10 hours of thermal exposure.

4. Conclusion

High-temperature thermal exposure at 1200 °C for 1 and 10 h significantly influenced the precipitate characteristics, microstructural stability, and mechanical performance of L-PBF-fabricated Fe–12Cr–6Al–1Ti–0.25Y_2O_3 alloys processed under a nitrogen atmosphere. Prolonged exposure led to precipitate coarsening, redistribution, and partial dissolution, accompanied by microstructural evolution. In the as-built condition, TiN and Y-rich precipitates were predominantly observed, whereas extended thermal exposure promoted the formation of complex Al–Y–O and Y–O–N precipitates. Mechanical testing revealed that a 1 h heat treatment resulted in a pronounced increase in ductility despite reductions in yield and ultimate tensile strengths, while further exposure to 10 h caused additional degradation in both strength and elongation.

REFERENCES

[1] S. Palaniappan, S. S. Joshi, S. Sharma, M. Radhakrishnan, K. V. M. Krishna, and N. B. Dahotre, “Additive manufacturing of FeCrAl alloys for nuclear applications - A focused review,” *Nucl. Mater. Energy*, vol. 40, no. January, p. 101702, 2024, doi: 10.1016/j.nme.2024.101702.

[2] O. Cakmak, H. Yeom, and J. Cho, “In-situ synthesis of TiN and its effects on Fe-12Cr-6Al in laser powder bed fusion,” *Addit. Manuf.*, vol. 84, no. April, p. 104148, 2024, doi: 10.1016/j.addma.2024.104148.

[3] L. L. Hsiung *et al.*, “Formation mechanism and the role of nanoparticles in Fe-Cr ODS steels developed for radiation tolerance,” *Phys. Rev. B - Condens. Matter Mater. Phys.*, vol. 82, no. 18, pp. 1–13, 2010, doi: 10.1103/PhysRevB.82.184103.

[4] J. Tang *et al.*, “Materials & Design Fabricating irradiation-tolerant ODS Fe-Cr steel with engineered Y-Ti-O nanoprecipitates by laser powder bed fusion,” *Mater. Des.*, vol. 262, no. January, p. 115466, 2026, doi: 10.1016/j.matdes.2026.115466.

[5] O. Cakmak, S. Lee, S. Gyu, D. Eo, H. Yeom, and J. W. Cho, “In-situ synthesis of nitrides and oxides through controlling reactive gas atmosphere during laser-powder bed fusion of Fe-12Cr-6Al,” *Mater. Des.*, vol. 240, no. October 2023, p. 112862, 2024, doi: 10.1016/j.matdes.2024.112862.

[6] S. Ukai, K. Sakamoto, S. Ohtsuka, S. Yamashita, and A. Kimura, “Alloy design and characterization of a recrystallized FeCrAl-ODS cladding for accident-tolerant BWR fuels : An overview of research activity in Japan,” *J. Nucl. Mater.*, vol. 583, no. February, p. 154508, 2023, doi: 10.1016/j.jnucmat.2023.154508.

[7] F. Villaret, X. Boulnat, P. Aubry, J. Zollinger, D. Fabrègue, and Y. de Carlan, “Modelling of delta ferrite to austenite phase transformation kinetics in martensitic steels: Application to rapid cooling in additive manufacturing,” *Materialia*, vol. 18, no. January, p. 101157, 2021, doi: 10.1016/j.mtla.2021.101157.

[8] Y. Zhang, H. Wang, H. Sun, and G. Chen, “Effects of annealing temperature on the microstructure, textures and tensile properties of cold-rolled Fe–13Cr–4Al alloys with different Nb contents,” *Mater. Sci. Eng. A*, vol. 798, no. September, p. 140236, 2020, doi: 10.1016/j.msea.2020.140236.

[9] I. A. Ovid’ko, R. Z. Valiev, and Y. T. Zhu, “Review on superior strength and enhanced ductility of metallic nanomaterials,” *Prog. Mater. Sci.*, vol. 94, pp. 462–540, 2018, doi: 10.1016/j.pmatsci.2018.02.002.